

Effect of Laser Shock Peening on the Microstructures and Properties of Oxide-Dispersion-Strengthened Austenitic Steels

Xueliang Yan, Fei Wang, Leimin Deng, Chenfei Zhang, Yongfeng Lu, Michael Nastasi, Marquis A. Kirk, Meimei Li, and Bai Cui*

Oxide-dispersion-strengthened (ODS) austenitic steels are promising materials for next-generation fossil and nuclear energy systems. In this study, laser shock peening (LSP) has been applied to ODS 304 austenitic steels, during which a high density of dislocations, stacking faults, and deformation twins are generated in the near surface of the material due to the interaction of laser-driven shock waves and the austenitic steel matrix. The dispersion particles impede the propagation of dislocations. The compressive residual stress generated by LSP increases with successive LSP scans and decreases along the depth, with a maximum value of -369 MPa. The hardness on the surface can be improved by 12% using LSP. In situ transmission electron microscopy (TEM) irradiation studies reveal that dislocations and incoherent twin boundaries induced by LSP serve as effective sinks to annihilate irradiation defects. These findings suggest that LSP can improve the mechanical properties and irradiation resistance of ODS austenitic steels in nuclear reactor environments.

properties.^[1] Most ODS steels have a ferritic steel matrix and few ODS steels are austenitic. ODS ferritic steels have been prevalently studied in the nuclear community leading to the development of many alloys such as 14YWT, 12YWT, MA956, MA957, and PM2000. ODS austenitic steels, such as ODS 316, ODS 310, and ODS 304, have been recently developed for next-generation fossil and nuclear energy systems, such as the very-high-temperature reactors (VHTR).^[2] Generally, austenitic steels have better creep resistance than ferritic steels, because the close-packed face-centered cubic (FCC) structure is more stable and more resistant to creep than the body-centered cubic (BCC) structure at high temperatures.^[3] On the other hand, ferritic steels have better void swelling resistance than austenitic steels, because the BCC structure results in a reduction of dislocation bias and increased

1. Introduction

Oxide-dispersion-strengthened (ODS) steels have a homogeneous dispersion of nanoscale oxide particles (e.g., $Y_2Ti_2O_7$ and Y_2TiO_5) in the steel matrix. Compared to conventional steels, ODS steels have improved thermomechanical and irradiation

self-diffusion, which are beneficial for reduced radiation swelling. The void swelling resistance of austenitic steels could be increased by the dispersion of oxide nanoparticles inside the matrix.^[4] The particle/matrix interfaces in ODS austenitic steels can act as nanoscale sinks for point defects, thus inhibiting void formation and increasing the void swelling resistance.^[5] In addition, oxide nanoparticles retard the motion of dislocations and reduce grain coarsening, thus increasing the mechanical strength and creep resistance of austenitic steels.

Laser shock peening (LSP) is a novel surface modification process, which has been used to improve the fatigue, wear, and stress corrosion cracking resistance of metallic materials such as stainless steels, aluminum, and titanium alloys.^[6] The LSP process utilizes high-energy laser pulses to irradiate the material surface to form a plasma (**Figure 1**). The explosive expansion of plasma generates shock waves that penetrate the bulk material and induce significant compressive residual stress in the range of 100 MPa–1 GPa.^[7] The depth of LSP-induced residual stresses depends on processing conditions and material properties, which generally ranges from 0.5 to over 1 mm.^[6] Compared to the traditional mechanical shot peening, LSP offers many advantages such as a deeper penetration and a higher magnitude of compressive stresses, a shorter process time, precise control, accuracy, and no contamination.^[8] The interaction of

Prof. B. Cui, Dr. X. L. Yan, F. Wang, Prof. M. Nastasi
Department of Mechanical & Materials Engineering, University of
Nebraska–Lincoln, Lincoln, NE 68588, USA
E-mail: bcui3@unl.edu

Dr. L. M. Deng, C. F. Zhang, Prof. Y. F. Lu
Department of Electrical Engineering, University of Nebraska–Lincoln,
Lincoln, NE 68588, USA

Prof. M. Nastasi
Nebraska Center for Energy Sciences Research, University of
Nebraska–Lincoln, Lincoln, NE 68588, USA

Prof. M. Nastasi, Prof. B. Cui
Nebraska Center for Materials and Nanoscience, University of
Nebraska–Lincoln, Lincoln, NE 68588, USA

Dr. M. A. Kirk, Dr. M. M. Li
Nuclear Engineering Division, Argonne National Laboratory, Argonne,
IL 60439, USA

 The ORCID identification number(s) for the author(s) of this article can be found under <https://doi.org/10.1002/adem.201700641>.

DOI: 10.1002/adem.201700641

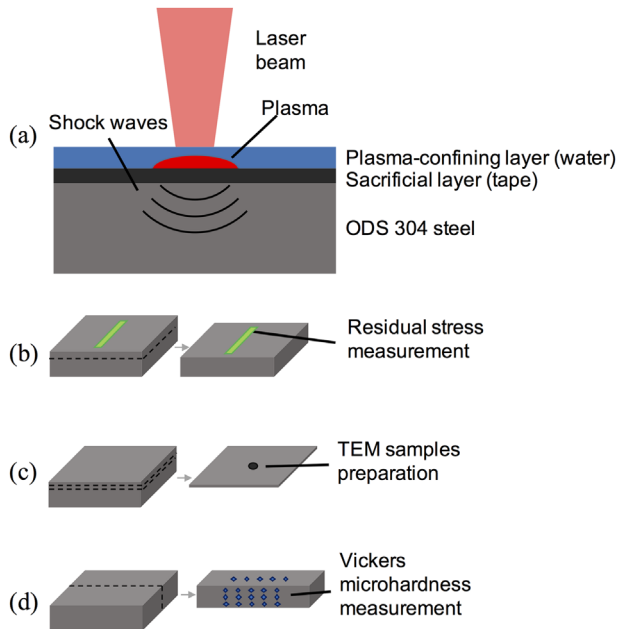


Figure 1. a) Schematic of the laser shock peening process on ODS 304 austenitic steels. b–d) Schematic of the residual stress measurement, TEM samples preparation, and Vickers hardness measurement, respectively.

laser-induced shock waves with metals can result in significant microstructural changes in the near surface of materials, such as an increased dislocation density, deformation twins, and phase transformation, depending on material properties and LSP conditions.^[9]

The improvement in mechanical and corrosion properties such as hardness, fatigue strength, stress corrosion cracking, and hydrogen embrittlement by LSP have been well documented in the literature.^[6,10] Recently, it is reported by our team that the microstructural changes by LSP are beneficial for improving the radiation resistance of austenitic stainless steels.^[11] The dislocations and incoherent twin boundaries can serve as high strength sinks for the annihilation of irradiation defects during 1 MeV Kr ion irradiation at room temperature. Consequently, the density of irradiation defects in LSP-treated 304 stainless steels becomes much lower than that in untreated steels.^[11a]

The benefits of LSP have been generally attributed to the effects of compressive residual stresses and plastic deformation, although the exact mechanisms remain unclear. This paper reports a comprehensive study of the effects of LSP processing on microstructures, residual stress, hardness, and irradiation resistance in ODS austenitic stainless steels. The primary objective is to understand the fundamental mechanisms that how LSP will modify the microstructures and improve the mechanical properties and irradiation behavior of this important material for the nuclear industry.

2. Experimental Section

The ODS 304 austenitic stainless steels were fabricated by two successive steps: mechanical alloying, and then spark

plasma sintering (SPS). The mixed powders included 70.65 wt% Fe (99.9%, <10 μm), 18 wt% Cr (99.2%, <10 μm), 8.5 wt% Ni (99.9%, 3–7 μm), 2 wt% W (99.9%, 1–5 μm), 0.5 wt% Ti (99.5%, <10 μm), and 0.35 wt% Y₂O₃ (99.995%, 25–50 nm), which were provided by Alfa Aesar. These powders were added into a 316 stainless steel grinding bowl with 316 stainless steel grinding balls (10 mm in diameter) in a glove box under an argon atmosphere with a ball-to-powder mass ratio of 5:1. The mixture of powders was milled at 250 rpm for 50 h using a high-energy planetary ball mill (Model Pulverisette 7, Fritsch GmbH). To prevent overheating, ball milling was interrupted every 50 min for a 20 min cooling. Consolidation of the mechanically alloyed powders was performed in an SPS system (Model SPS 10–4, Thermal Technologies) in a vacuum (2×10^{-2} Torr) at 1000 °C for 5 min under a pressure of 50 MPa. The powders were heated to the temperature at a rate of 100 °C min⁻¹. The sintered samples were 20 mm in diameter and several mm thick. The density was measured on a balance (AT201, Mettler Toledo) using the Archimedes method.

The microstructures of ODS 304 steel samples were characterized by electron backscattering diffraction (EBSD) and transmission electron microscopy (TEM). The sample surface for EBSD characterization was electrochemically polished in a solution of 5% HClO₄ and 95% C₂H₅OH. EBSD analysis was performed in a FEI Helios FIB/SEM 660 equipped with an EBSD detector (Hikari XP 2, AMETEK) with a step size of 0.01 μm. For the TEM sample preparation, 3 mm diameter disks were thinned to a thickness less than 100 nm by mechanical polishing. Final thinning to electron transparency was accomplished by electrochemical polishing in a twin jet polisher (TenuPol-5, Struers) using an electrolyte of 5% HClO₄ and 95% CH₃OH at –20 °C. Transmission electron microscopy was carried out in a JEOL 2010 LaB₆ operated at 200 kV using the diffraction-contrast bright-field (BF) and dark-field (DF) imaging modes. Energy dispersive spectroscopy (EDS) chemical analysis was performed using a Super-X windowless EDX detector in an FEI Tecnai Osiris S/TEM.

The LSP process of the ODS 304 steel samples is shown in Figure 1a. A Q-switched Nd:YAG pulse laser (PRII 8010, Continuum Electro-Optics) was used, with a pulse energy of 850 mJ, a wavelength of 1064 nm, a pulse duration of 7 ns, a repetition rate of 10 Hz, and a spot diameter of 1 mm. The power density was calculated as 15 GW cm⁻². The sample surface was coated with a black vinyl tape which acted as the sacrificial layer to avoid the laser ablation of the sample. A flowing film of deionized water covered the surface of black tape as the plasma-confining layer. The sacrificial layer and plasma-confining layer protected the working materials, which remained at room temperature during the LSP process, from laser heating. A square area of 10 × 10 mm was scanned by the laser beam with an overlap ratio of 50%.

The residual stresses in LSP-treated ODS 304 steels were measured using the sin²ψ method in an X-ray diffractometer (SmartLab, Rigaku) equipped with a monochromator to prevent the fluorescent effect, with Cu K_α radiation. Thin layers of the sample were successively removed by electrochemical polishing, with the surface successively scanned by X-rays to obtain the depth profile of the residual stresses, as shown in Figure 1b. Because the removal of each layer caused a redistribution of

residual stresses in the remaining specimen, the true stress distribution was corrected following the method developed by Moore and Evans.^[12] The near-surface microstructures of the ODS 304 steels were characterized by TEM. Disk samples of 3 mm diameter were cut from the region close to the surface (about 50 μm in depth), and then thinned to less than 100 μm from both sides by mechanical polishing, as shown in Figure 1c. Final thinning to electron transparency was accomplished by electrochemical polishing using an electrolyte of 5% HClO_4 and 95% CH_3OH at -20°C . Transmission electron microscopy was carried out in a JEOL 2010 LaB₆ operated at 200 kV using the diffraction-contrast BF imaging mode. The LSP-treated samples were cut into two halves along the cross section, and the Vickers microhardness was measured on top surface and cross section, as shown in Figure 1d, using a hardness tester (Tukon 2500, Wilson) with a load from 1 to 10 N and a dwell time of 10 s. The depth profile of hardness was measured along the cross section. The indent size is 20–30 μm and at least five indentations were measured to determine the hardness at each depth.

The in situ irradiation experiments were carried out at the IVEM-Tandem facility in Argonne National Laboratory, which consists of a Hitachi-9000 transmission electron microscope and a NEC implanter.^[11b,13] The TEM samples of LSP-treated ODS 304 steels were irradiated by 1 MeV Kr ions at room temperature. The accelerated Kr²⁺ ions bombarded the TEM sample at an incident angle of about $\approx 15^\circ$. Displacements per atom (dpa) were calculated by the Stopping and Range of Ions in Matter (SRIM) simulation using the Kinchin-Pease model and following the recommendations by Stoller et al.^[14] Under these irradiation conditions, a fluence of 5×10^{19} ions m^{-2} can cause a damage level of about 4 dpa. The accuracy of dose level is $\pm 10\%$.

3. Results

Microstructures of the as-fabricated ODS 304 austenitic steels were characterized by EBSD and TEM. Figure 2a is an inverse pole figure of the austenitic steel grain structure, which shows no preferred crystallographic orientation. The grain size ranges from 100 nm to 1.5 μm (Figure 2c), according to the statistic measurement in the EBSD images. The small grains of the ODS 304 steel were formed during the mechanical alloying process; the short heating time in SPS also limited the grain growth.^[15] Figure 2b is a BF-TEM image of the dispersion of nanoparticles, which are uniformly distributed in austenitic steel grains. Energy dispersive spectroscopy chemical analysis indicated that the nanoparticles were yttrium- and titanium-rich, suggesting that these were Y–Ti–O (presumably $\text{Y}_2\text{Ti}_2\text{O}_7$ and Y_2TiO_5), similar to other ODS austenitic steels.^[2a,2b] The majority of nanoparticles (more than 90%) were smaller than 10 nm (Figure 2d) according to the statistic measurements of the TEM images. The number density of the nanoparticles is $4.01 \times 10^{12} \text{mm}^{-3}$. The Y–Ti–O particles evolved from the Y_2O_3 particles (25–50 nm) during the mechanical alloying process. Recent research suggests that the

originally added Y_2O_3 powders are dissolved during the ball milling, and the oxygen-enriched Y–Ti–O nanoparticles precipitate during the annealing procedure.^[16] The precipitation of the nanoparticles initiates from the amorphous oxygen-rich regions formed during ball milling, as a consequence of the diffusion of dissolved Y_2O_3 as well as metal elements which have high affinity for oxygen such as Ti.^[17] The properties of these amorphous oxygen-rich regions determine the size and chemical composition of nanoparticles, which are crystallized during the SPS process.^[16c,18]

The magnitude of compressive residual stress generated by LSP is increased with the laser pulse energy and power density.^[11a,19] The LSP conditions used in this study were a laser pulse energy of 850 mJ and a power density of 15GWcm^{-2} , which are both the maximum for our Nd:YAG laser system. The compressive residual stresses can be also increased by successive LSP scans. Figure 3a shows the measured residual stress on the surface of ODS 304 steel samples as a function of the number of LSP scans. Note compressive stresses are expressed as negative values. Before LSP, the compressive residual stress on the surface of the sample was -29MPa , which was likely a result of mechanical polishing. The compressive residual stress on the surface increased with the number of LSP scans and became saturated after 20 LSP scans. The highest compressive stress was -369MPa . The saturation of the residual stress may be related to the saturation of plastic deformation in the subsurface microstructures (see Section 4, Discussion). The compressive residual stress across the treated area is in a relatively uniform biaxial in-plane distribution along the depth after a typical LSP treatment.^[6] The distribution of compressive residual stress along the depth of the samples after 6, 12, and 25 LSP scans is shown in Figure 3b. The magnitude of compressive residual stress was the highest on the surface, decreased gradually with the depth, and became zero at a depth of 400–500 μm . At the

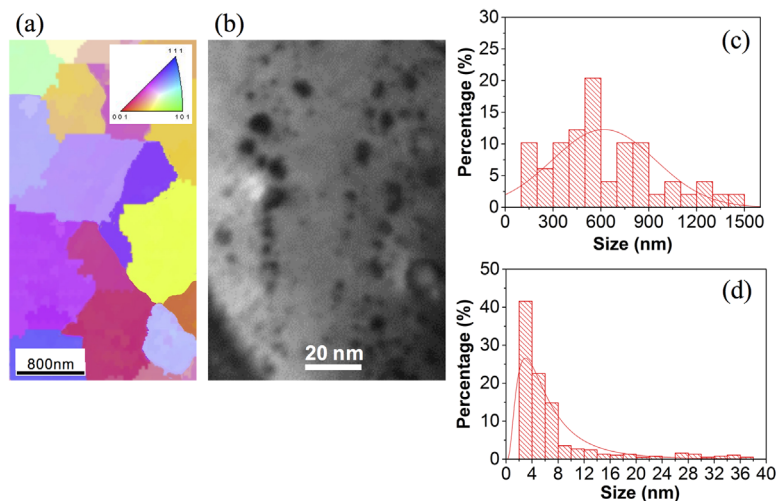


Figure 2. Microstructures of the as-fabricated ODS 304 austenitic steels. a) EBSD inverse pole figure of the grain structure. Inset: color key for crystallographic orientation. b) BF-TEM image of the dispersion of nanoparticles. c) Statistic distribution of the grain size with a Gaussian fitting curve. d) Statistic distribution of the particle size with a Gaussian fitting curve.

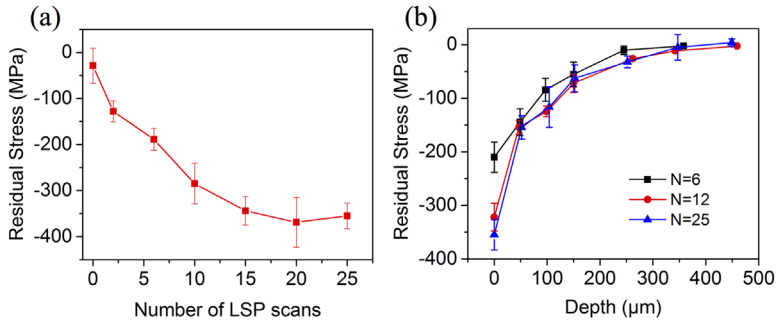


Figure 3. Compressive residual stress in LSP-treated ODS 304 steels. a) Residual stress on the surface as a function of the number of LSP scans. b) Residual stress distribution along the depth as a function of the number of LSP scans (N). The laser pulse energy is 850 mJ and the power density is 15 GW cm⁻².

same depth, the magnitude of compressive residual stress increased from 6 to 12 LSP scans, with a slight increase from 12 to 25 scans, which also indicates the saturation of compressive residual stress with the number of LSP scans.

The mechanical properties of the LSP-treated ODS 304 steels were evaluated by the Vickers indentation tests. **Figure 4a** shows that the hardness on the top surface of ODS 304 steel can be increased by successive LSP scans. It is noted that the saturation of hardness occurred at about 20 LSP scans, which is consistent with the saturation of the compressive residual stress. The highest hardness was 4.6 GPa at 20 LSP scans, which is 12% more than the untreated samples (4.1 GPa). The improvement of hardness can reflect the plastic deformation induced by LSP.^[6,20] **Figure 4b** shows the distribution of hardness along the depth of the sample after 25 LSP scans (red line). Compared with the distribution of compressive residual stress along the depth (**Figure 3b**), the hardness values have larger variations at each depth due to that the hardness was affected by the local microstructure changes such as grain size, grain orientation, grain boundaries, dislocations, and twins.^[21]

The microstructures in the near-surface region (about 50 μm in depth) of the LSP-treated ODS 304 steel were characterized by TEM (**Figure 5**). Compared to the untreated samples, there was no obvious change in the grain size and orientation of the austenitic steel matrix from TEM images. However, a high density of dislocations, stacking faults, and deformation twins were generated after LSP. The dislocation density was increased to $9.04 \times 10^{12} \text{ m}^{-2}$ compared to $2.32 \times 10^{11} \text{ m}^{-2}$ in the untreated samples, and the twin density was increased to $6.12 \times 10^{12} \text{ m}^{-2}$ compared to $1.57 \times 10^{11} \text{ m}^{-2}$ in the untreated samples. Stacking faults were formed by the dissociation of perfect dislocations in FCC austenitic steels.^[11a,22] The dislocations, stacking faults, and deformation twins indicated that significant plastic deformation occurred by the interaction

of laser-driven shock waves with the austenitic steel matrix during the LSP process. There was no evidence that the size or number density of dispersion particles was changed by LSP. In the ODS alloys, it is generally accepted that the incoherent dispersion particles are bypassed by dislocations via the Orowan mechanism at low temperatures (25–300 °C).^[23] That is, the dislocation line bows between the particle, and then moves forward leaving Orowan loops around the particle. It is important to note that **Figure 5d** shows two examples that are on the different steps of the dislocation-particle interaction process. The dislocation D1 is bowing the particle P1 and has not bypassed it. The dislocation D2 has almost bypassed

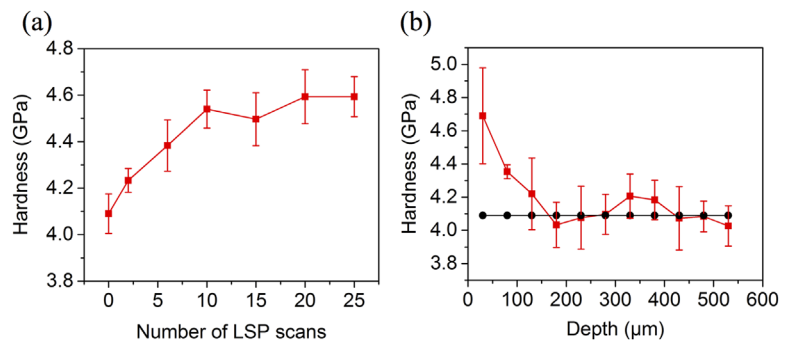


Figure 4. The hardness change of ODS 304 steel by LSP: a) hardness on the top surface as a function of the number of LSP scans; b) hardness distribution along the depth after 25 LSP scans (red line). The black horizontal line indicates the hardness of untreated sample. The laser pulse energy is 850 mJ and the power density is 15 GW cm⁻².

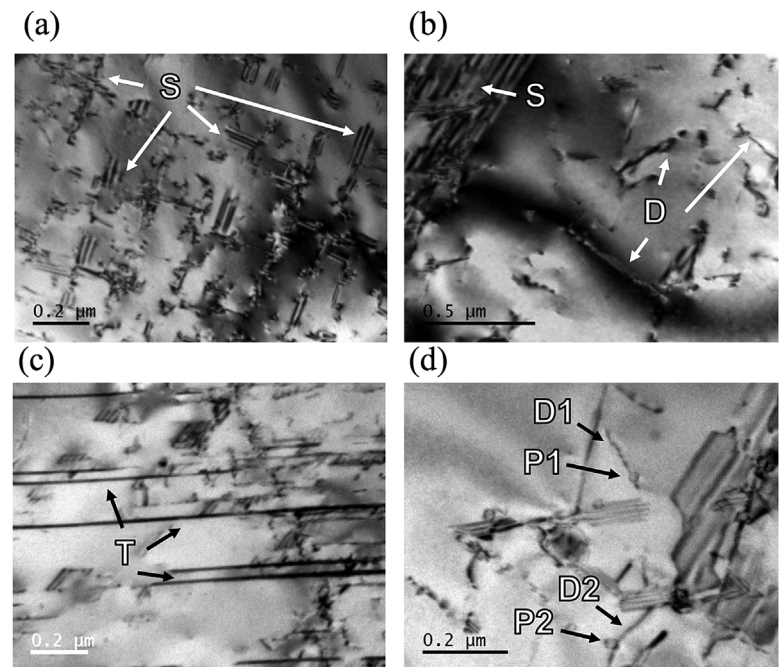


Figure 5. BF-TEM images of near-surface microstructures of ODS 304 steels after four LSP scans. S: stacking fault; D: dislocation line; T: deformation twin; P: dispersion particles.

the particle P2, but is still attached on the departure side of the particle P2. These two examples suggest that the dispersion particles act as the obstacles to impede the propagation of dislocations in ODS austenitic steels.

Two representative regions in the TEM samples of the LSP-treated ODS 304 steels were selected for in situ irradiation experiments: A region with dislocation lines (Figure 6) and another with deformation twin boundaries (Figure 7). Under 1 MeV Kr irradiation at room temperature, the dominant irradiation defect clusters formed in 304 steel samples are interstitial-type dislocation loops with Burgers vector $b=1/3\langle 111 \rangle$.^[24] The dislocation loops appear as bright dots under the DF imaging conditions in TEM.

Figure 6a and b show the DF and BF TEM images of an area in the LSP-treated ODS 304 steels with dislocation lines before irradiation. After the 1 MeV Kr irradiation of 0.17 dpa at room temperature, a large number of dislocation loops with several nanometers in diameter formed (Figure 6c). Two Regions 1 and 2 were selected for comparison, of which Region 1 has three dislocation lines while Region 2 has no dislocations. The dislocation loops in Region 1 and 2 are digitally highlighted for clarity. The number density of dislocation loops as a function of the irradiation dose in these two regions is presented in Figure 6d. The dislocation loop density is much lower in Region 1, and the difference became larger with the increasing dose. At 0.69 dpa, the dislocation loops density in Region 1 was about one-half in Region 2. This result suggests that dislocation lines generated by LSP are effective sinks for annihilating irradiation defects in ODS 304 steels.

To study the annihilation of irradiation defects by an incoherent twin boundary (ITB) generated by LSP (Figure 7a, b) in the ODS 304 steels, the evolution of dislocation loops in three regions, 1–3 in Figure 7c, is compared and measured as a function of irradiation dose. The dislocation loops in Region 1–3 are also digitally highlighted for clarity. The centers of these three regions, 1–3, have a distance of 15, 75, and 135 nm, respectively, from the ITB. The relationship between the number density of dislocation loops and irradiation dose is shown in Figure 7d. Region 1, which is closest to the ITB, has much fewer dislocation loops than Regions 2 and 3. This experimental result can be explained as that the irradiation defects in Region 1 could migrate to and annihilate at the ITB. However, the further the irradiation defects are away from the ITB, the longer the migration length to the ITB becomes and it becomes more difficult for the irradiation defects to be annihilated by the ITB. This is supported by the result that the dislocation loop density in Region 2 is much higher than Region 1, but is just slightly lower than Region 3.

4. Discussion

During the LSP process, the pressure of the laser-driven shock waves (typically several GPa^[25]) exceeds the dynamic yield strength of the ODS 304 stainless steel, thus plastic deformation with an extremely high strain rate (10^6 – 10^8 s⁻¹) occurs within a very short period of time (several tens of nanoseconds).^[26] The magnitude of the plastic strain decreases with the depth from the surface as the peak pressure of the shock wave attenuates along

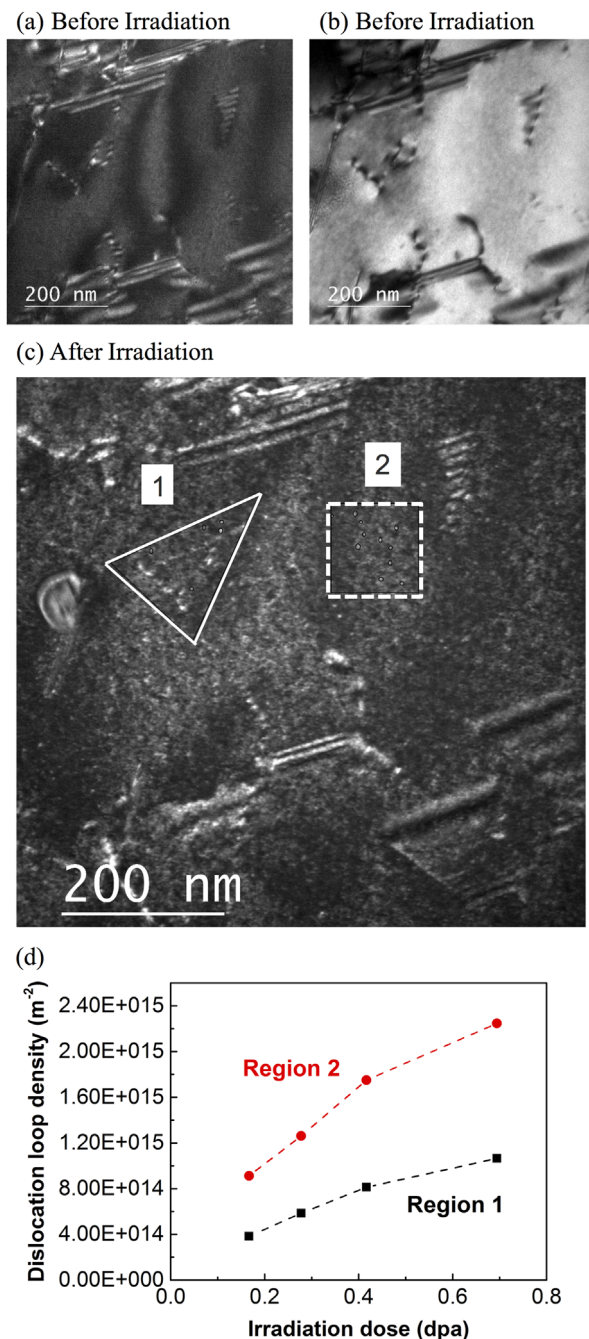


Figure 6. a) DF-TEM and b) BF-TEM images of an area with dislocation lines in LSP-treated ODS 304 steels before irradiation. c) DF-TEM image of the same area after an irradiation dose of 0.17 dpa. Region 1 has three dislocation lines while Region 2 has no dislocations. The dislocation loops in Region 1 and 2 are digitally highlighted for clarity. d) The number density of irradiation defect clusters (i.e., dislocation loops) as a function of irradiation dose within Regions 1 and 2 under 1 MeV Kr irradiation at room temperature.

the depth. Thus, after the shock wave passes, the residual plastic strain forms a compressive residual stress gradient under the surface, which is highest at the surface and decreases along the depth, as shown in Figure 3b. The compressive residual stress is

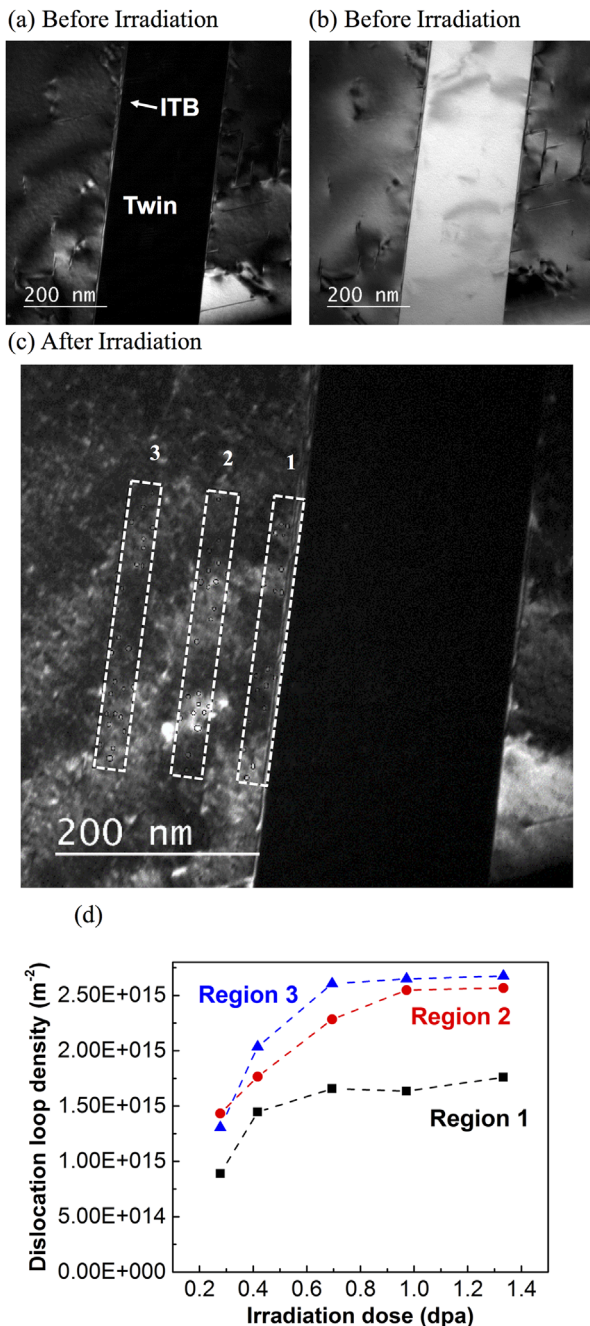


Figure 7. a) DF-TEM and b) BF-TEM images of an area with a deformation twin before irradiation. c) DF TEM image of the same area after an irradiation dose of 1.33 dpa. The centers of Regions 1–3 are 15, 75, and 135 nm, respectively, away from an incoherent twin boundary (ITB). The dislocation loops in Region 1–3 are also digitally highlighted for clarity. d) The number density of irradiation defect clusters (i.e., dislocation loops) as a function of irradiation dose within Regions 1 to 3 under 1 MeV Kr irradiation at room temperature.

saturated due to the saturation of plastic deformation, which is relevant to the yield strength of the material.^[27] In most materials, the maximum compressive residual stress achieved with LSP is close to -0.5 or $-0.6 \sigma_Y$, where σ_Y is the yield strength

of the target material.^[7a,26a] In this study, the maximum compressive residual stress on the surface was -369 MPa (Figure 3a), which was -0.53 of the yield strength of the ODS 304 stainless steel (about 700 MPa).^[28] This indicated that the compressive residual stress had been saturated in the ODS 304 steels with about 20 LSP scans.

During the interaction of laser-driven shock waves with the material, the kinetic energy of shock waves transforms into the plastic deformation energy, resulting in the rapid increase in the densities of dislocations, stacking faults, and deformation twins, which are typical features of plastic deformation in austenitic stainless steels.^[9] The generation and multiplication of dislocations can lead to work hardening, and twin boundaries also resist the dislocation slip.^[22] The maximum work hardening (indicated by the hardness) occurs on the surface where the LSP-induced plastic deformation is the highest, and then the plastic deformation decreases gradually with the depth. It is noted that the deformation microstructures, such as dislocations, stacking faults, and deformation twins, occur in the austenitic steel matrix. The dispersion particles have been observed to impede the dislocation motion (Figure 5d). Because the shear modulus of the dispersion particles (e.g., $G = 101$ GPa for $Y_2Ti_2O_7$)^[29] exceeds that of the 304 austenitic steel matrix ($G = 74\text{--}81$ GPa) and most dispersion particles form an incoherent interface with the matrix, dispersion particles may be bypassed by dislocations via the Orowan mechanism at room temperature.^[30]

The most common mechanical test to investigate the mechanical properties of LSP-treated materials is the hardness test, which reflects the effect of work hardening of LSP on the surface.^[31] Tensile testing is not applicable to these materials because LSP is a surface strengthening method and its effect is not suitable to be evaluated by a macroscale tensile test. The improvements of mechanical properties by LSP can be further evaluated by other mechanical tests depending on the engineering applications, such as fatigue, stress corrosion cracking, and erosion.^[6,10b,20] The improvement of these properties has been attributed to the effects of compressive residual stresses and microstructural changes, although the exact mechanisms remain unclear. It is possible that LSP could enhance the resistance of ODS austenitic steels to stress corrosion cracking and fatigue due to significant compressive residual stress; these studies are underway in our laboratory and will be the subject of a future manuscript.

In general, two strategies have been utilized to enhance the irradiation resistance of the materials: 1) developing inherent irradiation-tolerant materials; and 2) introducing stable high-strength sinks for the annihilation of irradiation defects.^[32] ODS alloys are promising irradiation-tolerant materials for Generation-IV nuclear power systems. Extensive TEM observations have shown that the particle/matrix interfaces in the ODS alloys act as nanoscale stable sinks for point defects generated during irradiation.^[33] In this study, LSP is shown to further improve the radiation resistance of the ODS austenitic steels by introducing defect sinks such as dislocations and incoherent twin boundaries. The number density of irradiation defects in the areas with dislocations and ITBs in LSP-treated ODS 304 steels is 30–50% of the untreated material. According to the number densities of dislocation lines and twins in the LSP samples and untreated

samples (Figure 5), and considering that the number densities of dislocation loops within a distance of 15 nm to the dislocation and twin boundary (Figure 6d, 7d) are about half of that in the regions without them, it is estimated that the irradiation defects could be decreased by 50% in about 5% of regions with dislocation lines in the LSP-treated ODS 304 steel samples compared with untreated samples, and in about 15% of regions with twins. Thus, the overall improvement of LSP on radiation resistance of ODS 304 steel is that the radiation-induced defects could be reduced by about 10%. A thorough discussion of the mechanisms of defect annihilation by these sinks in LSP-treated austenitic steels has been presented in our previous paper.^[11a] By introducing these high-strength defect sinks, irradiation hardening and Helium embrittlement can be suppressed because the irradiation-induced point defects and Helium atoms can be effectively captured by these sinks.^[34]

5. Conclusions

- 1) ODS 304 austenitic stainless steels were prepared by mechanical alloying and SPS, in which the majority of Y-Ti-O dispersion particles are smaller than 10 nm.
- 2) In the LSP process, the laser-driven shock waves induce intense plastic deformation in the ODS 304 austenitic steels. Consequently, a high density of dislocations, stacking faults, and deformation twins are generated in the near surface of the material. The dispersion particles impede the propagation of dislocations.
- 3) The compressive residual stress generated by LSP increases with successive LSP scans and decreases along the depth, with a maximum value of -369 MPa. The hardness on the surface can be improved by 12% using LSP, which also increases with successive LSP scans and decreases along the depth.
- 4) The LSP-induced dislocations and ITBs can serve as high strength sinks to annihilate the irradiation defect during the in situ ion irradiation. The number density of irradiation defects in the areas with dislocations and ITBs is 30–50% of the untreated material, which suggests LSP can improve irradiation resistance of ODS austenitic steels.

Acknowledgements

Acknowledgment is made to the donors of the American Chemical Society Petroleum Research Fund for support of this research. This work was partially supported by the Nebraska Public Power District through the Nebraska Center for Energy Sciences Research. Manufacturing and characterization analyses were performed at the NanoEngineering Research Core Facility (part of the Nebraska Nanoscale Facility), which is partially funded from the Nebraska Research Initiative. The electron microscopy with in situ ion irradiation was accomplished at Argonne National Laboratory at the IVEM-Tandem facility, a U.S. DOE facility funded by the DOE Office of Nuclear Energy, operating under Contract No. DE-AC02-06CH11357 by UChicago Argonne, LLC.

Conflict of Interest

The authors declare no conflict of interest.

Keywords

irradiation resistance, laser shock peening, microstructure, ODS austenitic steels, residual stress

Received: July 28, 2017
Revised: October 4, 2017
Published online: November 7, 2017

- [1] a) V. V. Sagaradze, V. I. Shalaev, V. L. Arbizov, B. N. Goshchitskii, Y. Tian, W. Qun, S. Jiguang, *J. Nucl. Mater.* **2001**, 295, 265; b) Z. Oksiuta, P. Mueller, P. Spätig, N. Baluc, *J. Nucl. Mater.* **2011**, 412, 221.
- [2] a) Y. Miao, K. Mo, Z. Zhou, X. Liu, K.-C. Lan, G. Zhang, M. K. Miller, K. A. Powers, Z.-G. Mei, J.-S. Park, *Mater. Sci. Eng. A* **2015**, 639, 585; b) H. Oka, M. Watanabe, N. Hashimoto, S. Ohnuki, S. Yamashita, S. Ohtsuka, *J. Nucl. Mater.* **2013**, 442, S164; c) R. R. Judkins, U. S. Rao, *Intermetallics* **2000**, 8, 1347; d) I. G. Wright, B. A. Pint, *Oak Ridge Natl. Lab. (ORNL)* **2008**.
- [3] W.-Y. Chen, Y. Miao, Y. Wu, C. A. Tomchik, K. Mo, J. Gan, M. A. Okuniewski, S. A. Maloy, J. F. Stubbins, *J. Nucl. Mater.* **2015**, 462, 242.
- [4] K. Mo, Z. Zhou, Y. Miao, D. Yun, H.-M. Tung, G. Zhang, W. Chen, J. Almer, J. F. Stubbins, *J. Nucl. Mater.* **2014**, 455, 376.
- [5] Y. Miao, K. Mo, Z. Zhou, X. Liu, K.-C. Lan, G. Zhang, M. K. Miller, K. A. Powers, J. F. Stubbins, *J. Nucl. Mater.* **2016**, 480, 195.
- [6] C. S. Montross, T. Wei, L. Ye, G. Clark, Y.-W. Mai, *Int. J. Fatigue* **2002**, 24, 1021.
- [7] a) R. A. Brockman, W. R. Braisted, S. E. Olson, R. D. Tenaglia, A. H. Clauer, K. Langer, M. J. Shepard, *Int. J. Fatigue* **2012**, 36, 96; b) R. Voothaluru, C. R. Liu, G. J. Cheng, *J. Manuf. Sci. Eng.* **2012**, 134, 061010.
- [8] a) Y. Al-Obaid, *Eng. Fract. Mech.* **1995**, 51, 19; b) P. P. Shukla, P. T. Swanson, C. J. Page, *Proc. Inst. Mech. Eng., Part B* **2014**, 228, 639.
- [9] a) J. Lu, K. Luo, Y. Zhang, G. Sun, Y. Gu, J. Zhou, X. Ren, X. Zhang, L. Zhang, K. Chen, *Acta Mater.* **2010**, 58, 5354; b) H. Ding, Y. C. Shin, *Comput. Mater. Sci.* **2012**, 53, 79; c) C. Ye, Y. Liao, S. Suslov, D. Lin, G. J. Cheng, *Mater. Sci. Eng., A* **2014**, 609, 195.
- [10] a) M. Kattoura, S. R. Mannava, D. Qian, V. K. Vasudevan, *Int. J. Fatigue* **2017**, 102, 121; b) P. Peyre, X. Scherpereel, L. Berthe, C. Carboni, R. Fabbro, G. Béranger, C. Lemaître, *Mater. Sci. Eng., A* **2000**, 280, 294.
- [11] a) Q. Lu, Q. Su, F. Wang, C. Zhang, Y. Lu, M. Nastasi, B. Cui, *J. Nucl. Mater.* **2017**, 489, 203; b) B. Cui, F. Wang, Q. Lu, *Microsc. Microanal.* **2016**, 22, 1474.
- [12] M. G. Moore, W. P. Evans, *SAE Trans.* **1958**, 66, 340.
- [13] a) D. Xu, B. D. Wirth, M. Li, M. A. Kirk, *Acta Mater.* **2012**, 60, 4286; b) M. Li, M. Kirk, P. Baldo, D. Xu, B. Wirth, *Philos. Mag.* **2012**, 92, 2048.
- [14] a) J. F. Ziegler, *J. Appl. Phys.* **1999**, 85, 1249; b) R. E. Stoller, M. B. Toloczko, G. S. Was, A. G. Certain, S. Dwaraknath, F. A. Garner, *Nucl. Instrum. Methods Phys. Res., Sect. B* **2013**, 310, 75.
- [15] V. Mamedov, *Powder Metall.* **2002**, 45, 322.
- [16] a) C. A. Williams, P. Unifantowicz, N. Baluc, G. D. W. Smith, E. A. Marquis, *Acta Mater.* **2013**, 61, 2219; b) M. Brocq, B. Radiguet, S. Poissonnet, F. Cuvilly, P. Pareige, F. Legendre, *J. Nucl. Mater.* **2011**, 409, 80; c) S. Yamashita, S. Ohtsuka, N. Akasaka, S. Ukai, S. Ohnuki, *Philos. Mag. Lett.* **2004**, 84, 525.
- [17] L. L. Hsiung, M. J. Fluss, S. J. Tumey, B. W. Choi, Y. Serruys, F. Willaime, A. Kimura, *Phys. Rev. B* **2010**, 82, 184103.
- [18] M. J. Alinger, G. R. Odette, D. T. Hoelzer, *Acta Mater.* **2009**, 57, 392.
- [19] F. Wang, C. Zhang, Y. Lu, M. Nastasi, B. Cui, *J. Am. Ceram. Soc.* **2017**, 100, 911.

- [20] A. Gujba, M. Medraj, *Materials* **2014**, 7, 7925.
- [21] E. Arzt, *Acta Mater.* **1998**, 46, 5611.
- [22] D. Hull, D. J. Bacon, *Introduction to Dislocations*, Elsevier, Oxford **2011**.
- [23] a) R. L. Klueh, P. J. Maziasz, I. S. Kim, L. Heatherly, D. T. Hoelzer, N. Hashimoto, E. A. Kenik, K. Miyahara, *J. Nucl. Mater.* **2002**, 307, 773; b) M. Bartsch, A. Wasilkowska, A. Czyrska-Filemonowicz, U. Messerschmidt, *Mater. Sci. Eng., A* **1999**, 272, 152.
- [24] a) J. I. Cole, S. M. Bruemmer, *J. Nucl. Mater.* **1995**, 225, 53; b) G. E. Lucas, *J. Nucl. Mater.* **1993**, 206, 287; c) Z. Jiao, J. T. Busby, G. S. Was, *J. Nucl. Mater.* **2007**, 361, 218.
- [25] P. Peyre, L. Berthe, X. Scherpereel, R. Fabbro, *J. Mater. Sci.* **1998**, 33, 1421.
- [26] a) R. Fabbro, P. Peyre, L. Berthe, X. Scherpereel, *J. Laser Appl.* **1998**, 10, 265; b) O. Hatamleh, *Int. J. Fatigue* **2009**, 31, 974.
- [27] K. Ding, *Surf. Eng.* **2003**, 19, 351.
- [28] M. A. Auger, V. de Castro, T. Leguey, A. Muñoz, R. Pareja, *J. Nucl. Mater.* **2013**, 436, 68.
- [29] L. F. He, J. Shirahata, T. Nakayama, T. Suzuki, H. Suematsu, I. Ihara, Y. W. Bao, T. Komatsu, K. Niihara, *Scr. Mater.* **2011**, 64, 548.
- [30] a) R. L. Klueh, P. J. Maziasz, I. S. Kim, L. Heatherly, D. T. Hoelzer, N. Hashimoto, E. A. Kenik, K. Miyahara, *J. Nucl. Mater.* **2002**, 307, 773; b) M. Bartsch, A. Wasilkowska, A. Czyrska-Filemonowicz, U. Messerschmidt, *Mater. Sci. Eng., A* **1999**, 272, 152.
- [31] a) Y. B. Guo, R. Caslaru, *J. Mater. Process. Technol.* **2011**, 211, 729; b) K. K. Liu, M. R. Hill, *Tribol. Int.* **2009**, 42, 1250.
- [32] G. R. Odette, M. J. Alinger, B. D. Wirth, *Annu. Rev. Mater. Res.* **2008**, 38, 471.
- [33] H. Kishimoto, M. J. Alinger, G. R. Odette, T. Yamamoto, *J. Nucl. Mater.* **2004**, 329–333, 369.
- [34] S. J. Zinkle, *Nucl. Instrum. Methods Phys. Res., Sect B* **2012**, 286, 4.